RSC Advances

ROYAL SOCIETY OF CHEMISTRY

www.rsc.org/advances

Cite this: DOI: 10.1039/c0xx00000x

www.rsc.org/advances

PAPER

Enhanced electrochemical performance and thermal stability of $CePO_4$-coated $Li_{1.2}Ni_{0.13}Co_{0.13}Mn_{0.54}O_2$ cathode material for lithium-ion batteries

J.J. Chen,[a,b] Z.D. Li,[a] H.F. Xiang,[*a] W.W. Wu,[a] S. Cheng,[c] L.J. Zhang,[d] Q.S. Wang,[d] Y.C. Wu [a]**

Received (in XXX, XXX) Xth XXXXXXXXX 20XX, Accepted Xth XXXXXXXXX 20XX

DOI: 10.1039/b000000x

Layered $Li_{1.2}Ni_{0.13}Co_{0.13}Mn_{0.54}O_2$ cathode is coated with $CePO_4$ layer via a simple precipitation method. The pristine and $CePO_4$-coated $Li_{1.2}Ni_{0.13}Co_{0.13}Mn_{0.54}O_2$ are characterized by X-ray diffraction (XRD), field-emission scanning electron microscopy (FE-SEM), high resolution transmission electron microscope (HR-TEM) and X-ray photoelectron spectroscopy (XPS), and results indicate that $CePO_4$ has been uniformly coated on the $Li_{1.2}Ni_{0.13}Co_{0.13}Mn_{0.54}O_2$. Charge-discharge tests show that the $CePO_4$-coated $Li_{1.2}Ni_{0.13}Co_{0.13}Mn_{0.54}O_2$ has an obviously enhanced electrochemical performance compared with the pristine sample: the initial coulombic efficiency from 88.26% to 92.19%, rate capability from 6 to 110 mAh g^{-1} at 10 C, high-temperature performance from 59.5 to 219.6 mAh g^{-1} at 55 °C after 20 cycles, and low-temperature performance from 128.3 to 246.7 mAh g^{-1} at -20 °C. According to the analysis from dc impedance and electrochemical impedance spectra, the improvements on the electrochemical performance are mainly because the coated $CePO_4$ layer can reduce side reactions of $Li_{1.2}Ni_{0.13}Co_{0.13}Mn_{0.54}O_2$ with the electrolyte, and thus form the cathode-electrolyte interface (CEI) layer with enhanced Li^+ diffusion. In addition, the $CePO_4$ layer significantly improves the thermal stability of the coexisting systems of charged cathode with the electrolyte. Therefore, $CePO_4$ coating will be a promising approach to improve the electrochemical performance and thermal stability of Li-rich layered oxide cathode materials.

Introduction

Developments of electric vehicles (EVs) and smart grids have the increasing demand for advanced rechargeable batteries, among which lithium-ion battery (LIB) is one of the most promising representatives because of its high energy density and successful commercialization in the portable electronic devices [1-3]. The energy density of the state-of-the-art LIBs is mainly governed by the electrode materials, especially the cathode materials [4-6]. In the widely used $LiCoO_2$|graphite [4] and $LiFePO_4$|graphite [5] cells, the capacity of the cathode materials (~140 mAh g^{-1}) is less than half of the graphite anode (~330 mAh g^{-1}) [6]. Therefore, the high-capacity candidates of the present cathode materials are needed to meet the demand for development of the advanced LIBs.

Li-rich layered oxide cathode materials, represented by $xLi_2MnO_3\cdot(1-x)LiMO_2$ (M = Ni, Co, Mn or combinations) can deliver a reversible capacity of ~250 mAh g^{-1}, which is quite attractive to high-energy LIBs for EVs and smart grid applications [7-9]. However, their drawbacks of large irreversible capacity loss during the initial cycle and poor rate capability limit the commercial utilization [10-14]. One of the main reasons for these drawbacks is the unsatisfying interface chemistry between this kind of cathode and common electrolytes [11]. The high capacity of Li-rich layered oxide cathode materials cannot be achieved until they are charged to an upper cut-off voltage above 4.5 V in order to activate Li_2MnO_3 component [12]. Such a high voltage is a rigorous challenge to the state-of-the-art carbonate-based electrolytes, and the electrolyte decomposition is unvoidably initiated by strongly oxidative charged electrodes and intermediate oxygen species [15]. In our previous paper [16], it is clearly indicated that the optimized cathode electrolyte interface (CEI) with the help of trimethyl phosphite (TMP) as the high-voltage electrolyte additive has the positive effects on improving the electrochemical performance and thermal stability of this kind of cathode material.

Besides the reformulation of the electrolytes, surface coating on the cathode material is the alternative effective method to modify the CEI film between the Li-rich layered oxide and the electrolyte [10,17-22]. Coated metal oxides [19-22] on the surface of the Li-rich layered oxide cathode can reduce initial irreversible capacity loss and enhance rate capability. Surface modification with metal phosphate was found to be more effective in lowering the irreversible capacity loss than that with Al_2O_3 due to the retention of more oxide ion vacancies in the lattice after the first charge [23]. Moreover, metal phosphates have the better thermal stability than its relevant metal oxide due to the strong covalent P-O bonding [23-26]. Recently, rare earth oxides have been coated on the surface of the Li-rich layered oxide cathode and the cycling performance has been improved [27,28], while their phosphates have seldom been considered. $CePO_4$ coating has been reported to improve the cycling stability of $LiCoO_2$ and $LiMn_2O_4$ at elevated temperature by suppressing Co or Mn dissolution [28-30]. Also, $CePO_4$ modification can improve the rate capability of $LiFePO_4$/C, because $CePO_4$ as an ionic conductor with stable structure can reduce side reactions and enhances migration of the lithium-ions at the electrode/electrolyte interface [31].

Herein, we performed the $CePO_4$ coating on the $0.5Li_2MnO_3\cdot0.5LiNi_{1/3}Co_{1/3}Mn_{1/3}O_2$ cathode (denoted as $Li_{1.2}Ni_{0.13}Co_{0.13}Mn_{0.54}O_2$, and abbreviated as LNCMO) by a simple precipitation reaction. After the structures of the cathode materials with and without coating have been indentified, the effects of $CePO_4$ coating on the electrochemical performance and thermal stability of the Li-rich layered oxide cathode are systemically investigated. Definitely, compared with the pristine LNCMO, the $CePO_4$-coated $Li_{1.2}Ni_{0.13}Co_{0.13}Mn_{0.54}O_2$ (abbreviated as CP-LNCMO) shows an obvious improvement on

initial coulombic efficiency, rate capability, high-temperature and low-temperature performance.

Experimental

Materials synthesis

The pristine LNCMO was prepared by a co-precipitation method, as described previously [16]. Surface coating of LNCMO with $CePO_4$ were carried out as follows: $Ce(NO_3)_3{\cdot}6H_2O$ (54.9 mg) and $(NH_4)_2HPO_4$ (16.8 mg) were dissolved in distilled water until a white suspension (of $CePO_4$) was obtained. The pristine LNCMO powder was then added to the suspension and was magnetically stirred for 20 min to form a slurry. The weight ratio of $CePO_4$ and LNCMO was 3:100. Subsequently, the slurry was dried in an oven for 12 h at 100 ^oC, and annealed at 400 ^oC for 5 h in a furnace to obtain the CP-LNCMO.

Characterization and electrochemical measurements

The crystalline structures of the pristine LNCMO and CP-LNCMO were identified by X-ray diffraction (XRD) using a diffractometer (D/MAX2500 V, Cu Ka radiation). The diffraction patterns were recorded in the 2 theta range from 10° to 80°. The particle size and morphology of the pristine LNCMO and CP-LNCMO were observed by field-emission scanning electron microscopy (FE-SEM, Hitachi SU8020) and high resolution transmission electron microscope (HR-TEM, JEM-2100F). X-ray photoelectron spectroscopy (XPS, ESCALAB250) was performed to characterize the surface state of the obtained products.

The electrochemical performances of the pristine LNCMO and CP-LNCMO were investigated using CR2032 coin-type cells assembled in an argon-filled glove box (MBraun). In order to make the electrode laminate, a slurry containing 84 wt.% active material, 8 wt.% acetylene black and 8 wt.% polyvinylidene fluoride (PVDF) dispersed in N-methyl-2-pyrrolidinone (NMP) was cast onto an aluminum current collector. After vacuum drying at 70 ◦C, the laminate was punched into discs (Φ14 mm) for assembling the coin cells. The mass loading in the electrode was controlled at about 2.5 mg cm^{-2}. Celgard 2400 microporous polypropylene membrane was used as separator. Highly pure lithium foil was used as the counter electrode and reference electrode for the cell assembly. The electrolyte was 1 M $LiPF_6$/ethylene carbonate (EC) + dimethyl carbonate (DMC) (1:1 w/w). The cell performance of the pristine LNCMO and CP-LNCMO were evaluated on a multichannel battery cycler (Neware BTS2300). All the cells were initially cycled twice between 2.5 and 4.8 V at a current rate of 0.1 C (1 C=200 mA g^{-1}). Then the cycling tests were performed at a current rate of 0.5 C in the constant current-constant voltage (CC-CV) charge mode and constant current (CC) discharge mode between 2.5 and 4.6 V. For the high temperature tests, the cells were galvanostatically cycled between 2.5 and 4.6 V at 55 ^oC at a current rate of 0.5 C. For the low temperature tests, the cells were galvanostatically charged to 4.6 V at room temperature then discharged at 0 ^oC or -20 ^oC at a current rate of 0.1 C. Cyclic voltammograms (CV) were performed over the potential range of 2.5-4.8 V at a scanning rate of 0.2 mV s^{-1} on a CHI 604D electrochemical workstation (Shanghai Chenhua Instruments Co. Ltd.). The electrochemical impedance spectra of the cells were also measured on the CHI electrochemical workstation with the frequency range and potential perturbation set as 1 MHz to 0.01 Hz and 10 mV at the state of charge (SOC) of 50%. The internal resistance of the cells was measured by a current interruption technique. This was done by cutting off the current intermittently for 1 min through the process of charge and recording the voltage change after interruption. Thus, the dc impedance of a cell (R_{dc}) can be calculated as $R_{dc} = \Delta U/\Delta I$, where ΔU is the difference between the voltage of before and after the 1-min interruption [32]. Thermal stability of the coexisting systems of the charged LNCMO and CP-LNCMO cathode with electrolyte was evaluated by using a Calvet-type calorimeter (Setaram C80). 23 mg cathode materials (after charged to 4.6 V in the cells and disassembled in the glove box) and 50 mg electrolyte were placed in a high-pressure stainless steel vessel with dry argon atmosphere. The measurement was performed at a heating rate of 0.2 ^oC min^{-1} from room temperature to 300 ^oC, and the C80 calculations were based on the weight of the electrolyte. More details can be found in our previous report [33]. All the testing above was performed at room temperature unless otherwise specified.

Results and discussion

The XRD patterns of the pristine LNCMO and CP-LNCMO samples are shown in **Fig. 1**. All the major diffraction peaks can be indexed as a layered oxide lattice based on a hexagonal α-$NaFeO_2$ type structure with a space group R-3m [18]. Both (006)/(102) and (108)/(110) doublets are clearly split, suggesting that the material crystallized in the layered structure without formation of any spinel structure [23]. The weak peaks between 20° and 25° (marked by *) are reflected by a monoclinic unit cell with a C2/m symmetry, due to a $LiMn_6$ cation arrangement that occurs in the transition metal layers of Li_2MnO_3 region. No peak of $CePO_4$ is observed due to its low quantity, illustrating that the coating processes do not destroy the structure of the Li-rich layered oxides and no impurity appears in the XRD patterns.

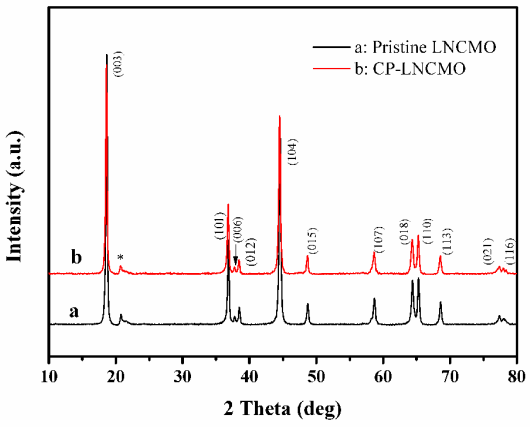

Fig. 1 XRD patterns of the pristine LNCMO and CP-LNCMO.

The morphologies of the pristine LNCMO and CP-LNCMO samples were investigated by FE-SEM, as shown in **Fig. 2**. From **Fig. 2a** and **2c**, the pristine LNCMO spherical particles are 2-10 μm in diameter. As shown in **Fig. 2b** and **2d**, the surface of the CP-LMNCO is coated by $CePO_4$ particles, and becomes rough. From the FE-SEM results, we expect that $CePO_4$ coating of LNCMO can effectively decrease the direct contact area between the high-voltage cathode material and the electrolyte. **Fig. 3** shows the HRTEM images of the pristine LNCMO and CP-LNCMO particles. Compared with the surface of the pristine LNCMO (**Fig. 3a**), the surface of CP-LNCMO is quite rough and scatted by $CePO_4$ particles (**Fig. 3b**). The distance between two

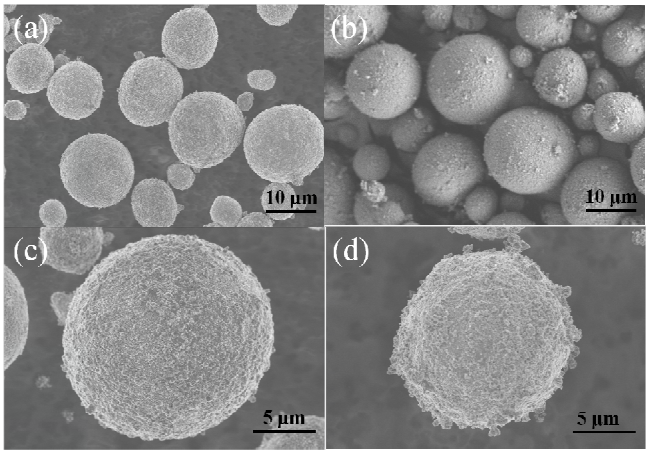

Fig. 2 SEM images of (a) the pristine LNCMO and (b) CP-LNCMO at low magnification (2.0k ×), (c) the pristine LNCMO and (d) CP-LNCMO at high magnification (5.0k ×).

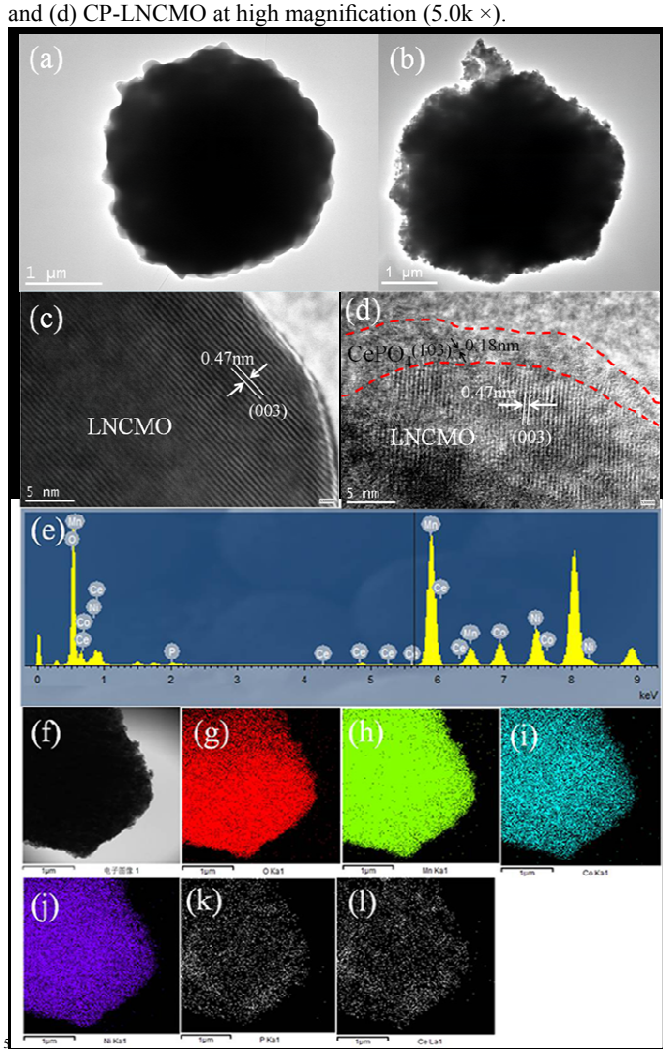

Fig. 3 TEM images of the pristine LNCMO (a, c) and CP-LNCMO (b, d), the EDS (e) and maps (f-l) of the CP-LNCMO.

lattice fringes of the pristine LNCMO is calculated to be 0.47 nm, which is assigned to (003) plane of LNCMO (**Fig. 3c**). In **Fig. 3d,** the distances between two lattice fringes on the internal and surface of the CP-LNCMO are 0.47 nm and 0.18 nm, assigned to (003) plane of LNCMO and (103) plane of $CePO_4$, respectively, implying that the $CePO_4$ coating processes do not destroy the structure of the Li-rich layered oxides (in agreement with the XRD results) and the coated $CePO_4$ is crystalline. EDS analysis is performed and the results are shown in **Figs. 3e-l**. The EDS analysis (**Fig. 3e**) reveals the presence of Ni, Co, Mn, O, Ce and P in the CP-LNCMO sample. The EDS element maps (**Figs. 3f-l**) clearly reveal that the Ce and P elements in the composite are uniformly distributed on the surface of LNCMO particles, illustrating that the $CePO_4$ is homogenously coated on the surface of LNCMO particles.

The XPS spectra of the pristine LNCMO and CP-LNCMO samples are shown in **Fig. 4**. As shown in **Fig. 4a**, the two peaks at 902.4 and 897.4 eV are assigned to Ni $2p_{1/2}$ [34,35] on the surface of the prisine LNCMO. After coating $CePO_4$, in **Fig. 4b**, the signal at 901.1 eV (assigned to Ce $3d_{3/2}$) is characteristic of Ce^{3+} [36,37]. The XPS results indicate that it is Ce (III) spectrum that is detected and definitely the coating layer is $CePO_4$, combined with EDS results.

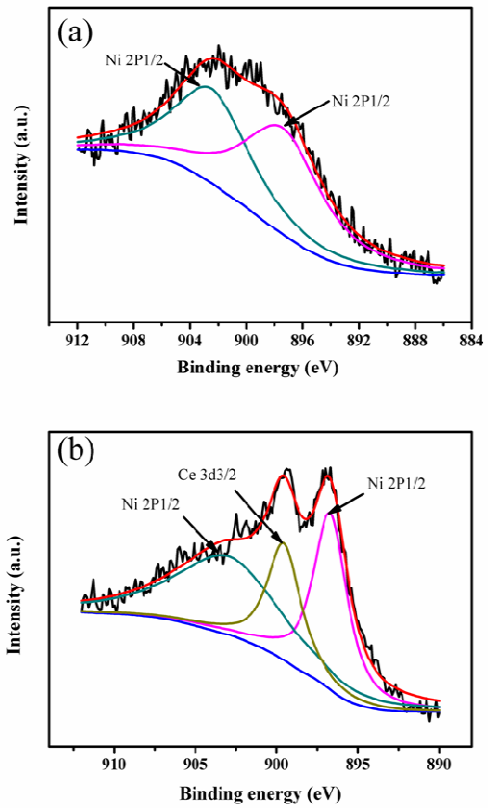

Fig.4 XPS of the pristine LNCMO (a) and CP-LNCMO (b).

Fig. 5 shows the CV profiles of the pristine LNCMO and CP-LNCMO. By comparing the pristine LNCMO with the CP-LNCMO, the anodic/cathodic behaviors are quite similar. During the first cycle, the anodic peaks of both simples are located at about 4.2 V which is associated with Ni^{2+} and Co^{3+} oxidation processes, while the second anodic peaks at above 4.5 V is predominantly associated with oxygen release and Li^+ extraction from the Li_2MnO_3 component [38]. For the CP-LNCMO sample, the peak shifts to lower potential and around 4.1 V during the following two cycles. Such relatively low oxidation potential is beneficial to the effective Li^+ extraction in the cathode-active material after the $CePO_4$ coating. Furthermore, in the cathodic

process, despite the broad slope above 3.5 V related to the reductions of $Ni^{4+} \rightarrow Ni^{2+}$ and $Co^{4+} \rightarrow Co^{3+}$, the apparent 3.1 V peak must be associated with the partial reduction of Mn^{4+} to Mn^{3+} in the transformed $Li_{1-x}MnO_2$ [39]. Compared with the pristine LNCMO, the cathodic curves of the CP-LNCMO are more repeatable, implying that the coated $CePO_4$ restrains LNCMO structural evolution.

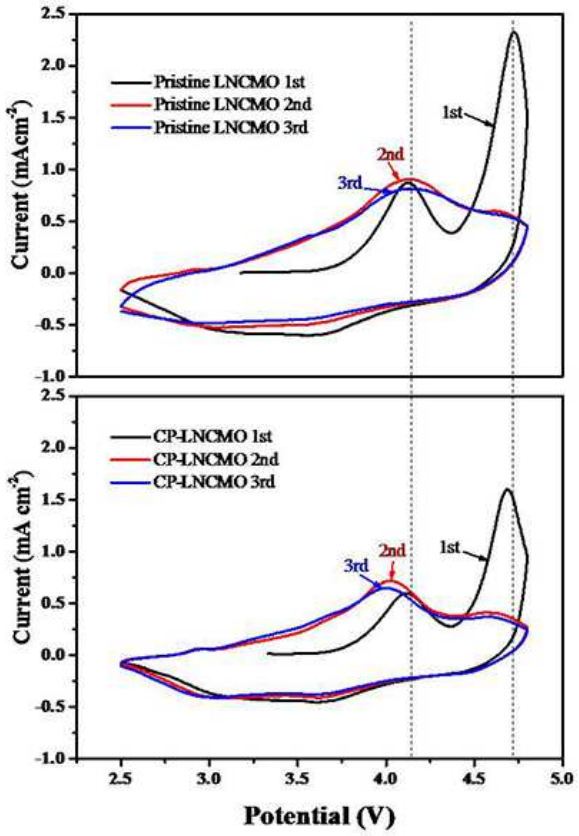

Fig. 5 Cyclic voltammetry of the pristine LNCMO and CP-LNCMO electrodes at 0.2 mV s^{-1} scan rate.

The initial charge-discharge curves and the cycling performance of the pristine LNCMO and CP-LNCMO samples are shown in **Fig. 6**. As shown in **Fig. 6a**, the initial charge and discharge capacities for the pristine LNCMO are 302 and 267 mAh g^{-1} at 0.1 C, respectively. So the irreversible capacity is 35 mAh g^{-1} and coulombic efficiency is 88.26%. As for CP-LNCMO, the initial charge and discharge capacities are 305 and 281 mAh g^{-1}, respectively. Therefore, CP-LNCMO has the lower irreversible capacity of 23 mAh g^{-1} and higher coulombic efficiency of 92.19% than the pristine LNCMO. This should be attributed to the suppressed side reactions between the electrolyte and the LNCMO cathode by $CePO_4$ coating. **Fig. 6b** shows the cycling performance of the pristine LNCMO and the CP-NCMO. After two formation cycles at 0.1 C, the discharge capacities of the pristine LNCMO are about 230, 203 and 191 mAh g^{-1} at the 3rd, 50th and 80th cycle at 0.5 C, whereas those of CP-LNCMO are about 240, 213.5 and 201 mAh g^{-1} at the 3rd, 50th and 80th cycle, respectively. These results suggest that the coated $CePO_4$ effectively improved the cycling stability of LNCMO and bulk structure revolution have been restained.

It is widely reported that the rate capability of Li-rich layered oxide cathode is poor, which becomes one of main drawbacks of this material for the commercial utilization [10]. The poor rate capability is usually ascribed to the formation of a high-resistance CEI layer on the cathode surface owing to electrolyte oxidation at high potentials [15,16]. **Fig. 7** shows rate

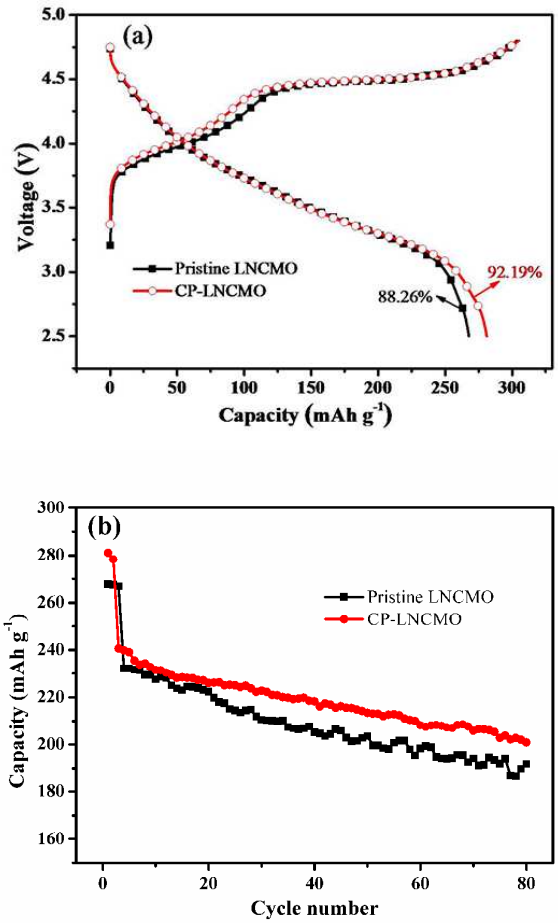

Fig. 6 Initial voltage profiles of the pristine LNCMO and CP-LNCMO electrodes at 0.1 C (a), cycling performance of both electrodes at 0.5 C (b).

capability of the pristine LNCMO and the CP-LNCMO. After two formation cycles at 0.1 C, the discharge capacities of the pristine LNCMO and the CP-LNCMO are comparative at 0.5 C. When the current rates increase to 1 C, 2 C, 5 C and 10 C, the discharge capacities of the pristine LNCMO, rapidly drop to 171, 103, 48 and 6 mAh g^{-1}, respectively. However, for the CP-LNCMO, the discharge capacities are 231, 205, 172 and 110 mAh g^{-1} at 1 C, 2 C, 5 C and 10 C, respectively. That is, the rate capability of LNCMO can be remarkably improved by the $CePO_4$ coating. In addition, when the current rate returns back to 0.5 C, the discharge capacities of both samples can be restored.

At elevated temperatures, Mn and Co dissolutions from LNCMO result in serious capacity fading during charge and discharge [29]. **Fig. 8** reveals the cycling performance of the pristine LNCMO and the CP-LNCMO cathodes at elevated temperature. After two formation cycles at room temperature, the initial discharge capacities at 55 °C of the pristine LNCMO and CP-LNCMO are 241.1 and 280.8 mAh g^{-1}, respectively. After 20 cycles, the capacity of the pristine LNCMO rapidly fades to 59.6 mAh g^{-1}, with the low capacity retention of 24.7%. However, the CP-LNCMO still keeps a quite high capacity of 219.6 mAh g^{-1}, and the capacity retention is as high as 78.2%. In order to figure out the reason for the improvement on high-temperature capacity

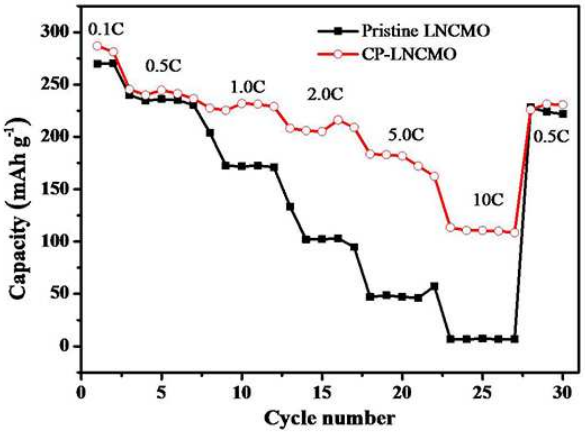

Fig. 7 Rate capability of the pristine LNCMO and CP-LNCMO electrodes.

retention from the $CePO_4$ coating, both the pristine LNCMO and the CP-LNCMO electrodes were soaked in 6 g electrolyte and stored at 55 °C. After 60 h, as shown in the insets of **Fig. 8**, the electrolyte stored with the pristine LNCMO became light brown, while that with the CP-LNCMO electrode was still colorless. The color change of the former is probably due to the dissolution of Mn and Co into the electrolyte at 55 °C. Therefore, it can be concluded that the coated $CePO_4$ can effectively prevent Mn and Co ions from dissolving into the electrolyte at elevated temperature, and improve the high-temperature cycling stability of the LNCMO.

Up to now, low-temperature performance of LIBs keeps a big challenge to meet the requirements of EVs, because of the decrease in the both discharge capacity and voltage plateau [40]. To the best of our knowledge, low-temperature performance of Li-rich layered oxide cathode materials has seldom been investigated in previous literatures. Here, we compare the low-temperature performance of the pristine LNCMO and the CP-LNCMO cathodes at 0 °C and -20 °C, as shown in **Fig. 9**. For the pristine LNCMO, the discharge capacities are 234.7 mAh g^{-1} at 0 °C and 128.3 mAh g^{-1} at -20 °C. However, the CP-LNCMO can deliver the discharge capacities of 278.5 at 0 °C and 246.7 mAh g^{-1} at -20 °C, respectively. As far as the capacity retention at low temperature is concerned, the discharge capacities of the pristine LNCMO and CP-LNCMO at -20 °C are 44.8% and 83.1% of the corresponding capacities at room temperature, respectively. In addition, the discharge voltage plateau of the CP-LNCMO is higher than that of the pristine LNCMO at the same temperatures. Therefore, the low-temperature performance of the LNCMO can be significantly improved by the $CePO_4$ coating. Herein, since the main difference is on the CEI interface, the improved low-temperature performance of CP-LNCMO is resulted from the optimized CEI interface by the $CePO_4$ coating.

To further understand the electrochemical processes in the CP-LNCMO, dc resistance is tested. As shown in **Fig. 10**, the dc resistance measurements show that the CP-LNCMO has a lower dc resistance than the pristine LNCMO, especially at high potential (> 4 V). We speculate that the lower dc resistance results from the coated $CePO_4$ layer, which can suppress the electrochemical reactions between the electrolyte and charged LNCMO cathode. Furthermore, **Fig. 11** shows that the Nyquist plots of the pristine LNCMO and CP-LMNCO electrodes at the SOC of 50% after the 3rd and 100th cycle, respectively. EIS results were fitted by using an equivalent circuit, in which R_e, R_f, R_{ct} and W stand for internal resistance of the cell, the impedance of Li^+ diffusion in the interface (herein CEI) film, the impedance

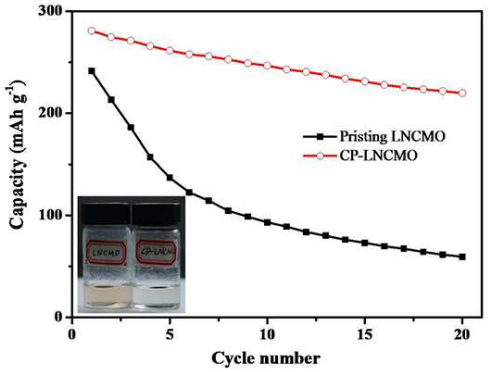

Fig. 8 Capacity retention of the pristine LNCMO and CP-LNCMO electrodes at 55 °C, the insets show both electrodes stored in the electrolyte at 55 °C for 60 h.

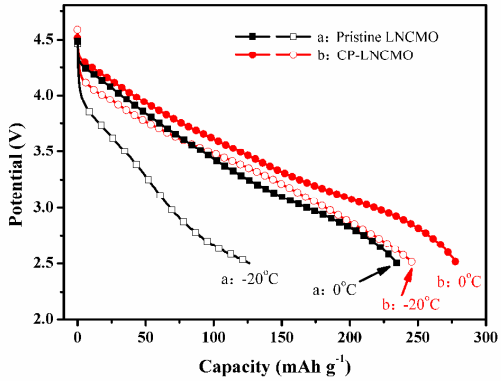

Fig. 9 Discharge curves of the pristine LNCMO and CP-LNCMO electrodes at low temperatures.

of charge transfer and Warburg impedance, respectively [41,42]. The fitted impedance parameters of the equivalent circuit are listed in **Table 1**. The values of R_e of the CP-LNCMO are relatively smaller than those of the pristine LNCMO at the same cycle, which suggests that the $CePO_4$ coating can reduce the negative effect on the electrolyte from the LNCMO cathode. The values of R_f of the pristine LNCMO are 236.8 and 270.4 Ω, much higher than those of the CP-LNCMO (84.2 and 199.5 Ω) after the 3rd and 100th cycle, respectively. This result supports that the coated $CePO_4$ suppresses the growth of CEI film on the LNCMO cathode. The values of R_{ct} of pristine LNCMO drastically increase from 276.7 to 867.4 Ω, while those of the CP-LNCMO show negligible change from 105.8 Ω at the 3rd cycle to 103.8 Ω at the 100th cycle. Herein, the low and stable charge transfer impedance suggests that the coated $CePO_4$ layer can reduce side reactions of LNCMO with the electrolyte, and thus form the CEI layer with enhanced Li^+ diffusion [12], which is the main reason for the improvement of the $CePO_4$ on the electrochemical performance of the LNCMO. XPS results of the electrodes after two formation cycles also support the point that $CePO_4$ coating can minimize the electrolyte decomposition at high voltage and suppress the growth of CEI film. In **Fig.12**, because of the

protection of the coated $CePO_4$, the CP-LNCMO electrode has the decreased C 1s peak and the enhanced Mn 2p3/2 peak, which indicate less CEI formation and Mn dissolution.

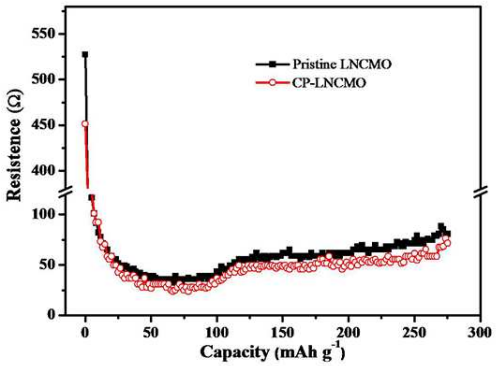

Fig. 10 Relationship between special capacity and dc resistance of the pristine LNCMO and CP-LNCMO electrodes.

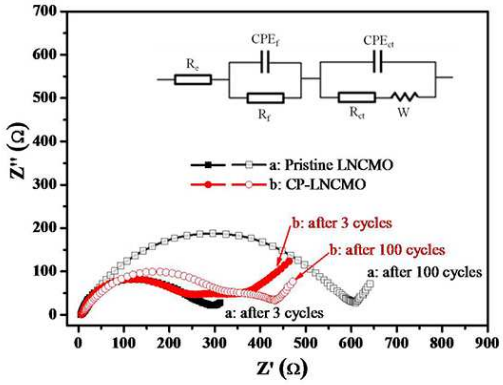

Fig. 11 EIS results of the pristine LNCMO and CP-LNCMO electrodes, the inset shows equivalent circuit for Nyquist plots.

Table 1 Fitted impedance parameters of the pristine LNCMO and CP-LNCMO.

Sample	R_e (Ω)	R_f (Ω)	R_{ct} (Ω)	W (S $sec^{1/2}$)
Pristine LNCMO (3^{rd})	6.8	236.8	276.7	0.02839
Pristine LNCMO (100^{th})	8.5	270.4	867.4	0.02097
CP-LNCMO (3^{rd})	4.6	84.2	105.8	0.08808
CP-LNCMO (100^{th})	7.3	199.5	103.8	0.05458

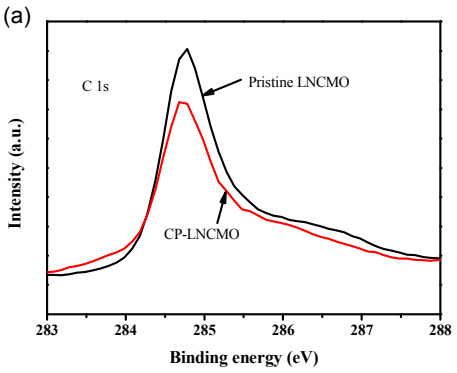

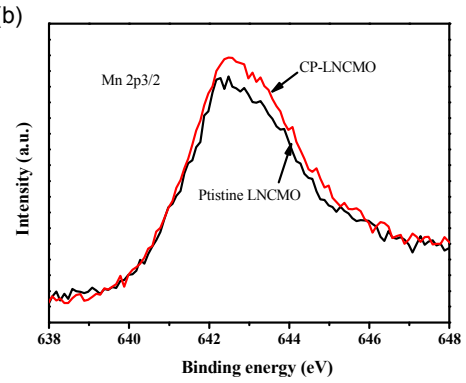

Fig. 12 XPS spectra of the pristine LNCMO and CP-LNCMO electrodes after 2 formation cycles.

Fig. 13 shows the C80 heat flow curves of the charged pristine LNCMO and CP-LNCMO cathode materials with the electrolyte. As we reported previously [33], the maximal heat flow and its corresponding temperature both have very important effect on the thermal stability of LIBs. Herein, the system with the CP-LNCMO has an onset exothermic temperature of 185 °C, higher than that (160 °C) of the system with the pristine LNCMO. Meanwhile, the main exothermic peak of the system with the CP-LNCMO was delayed to 211 °C from 182 °C of the pristine LNCMO. In conclusion, all the C80 results support the viewpoint that $CePO_4$ coating has significantly enhanced the thermal stability of the coexisting systems of charged LNCMO cathode and the electrolyte.

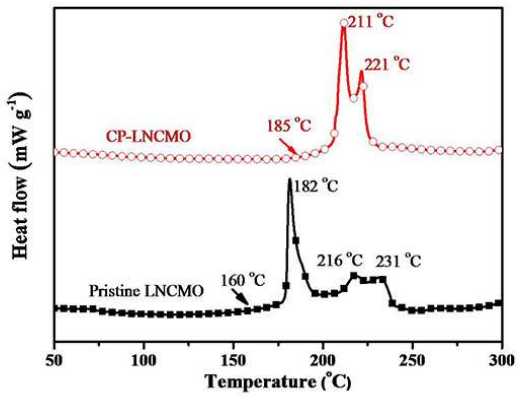

Fig. 13 C80 heat flow curves of coexistence systems of 50 mg electrolyte and 23 mg charged cathode materials (charged to 4.6 V) at a heating rate of 0.2 °C min^{-1}.

Conclusions

$CePO_4$ was uniformly coated on the surface of the Li-rich layered oxide $Li_{1.2}Mn_{0.54}Ni_{0.13}Co_{0.13}O_2$ particles via a simple precipitation method. The coated $CePO_4$ can not only suppress the side reactions between the cathode and the electrolyte, but also increase the Li^+ migration rate at the interface and improve the thermal stability of the coexisting systems of the charged LNCMO cathode and the electrolyte. As a result, the rate capability, high-temperatue and low-temperatue performance of

the LNCMO have been significantly improved from $CePO_4$ coating. The Li-rich layered cathode with uniformly $CePO_4$ layer coated by a simple and effective method could be a significant breakthrough in the development of advanced LIBs with higher energy, longer cycle life and stronger safety.

Acknowledgements

This study was supported by National Science Foundation of China (Grant Nos. 21006033, 51372060 and 51176183) and the Fundamental Research Funds for the Central Universities (2013HGCH0002).

Notes and references

[a] School of Materials Science and Engineering, Hefei University of Technology, Anhui Hefei, 230009, PR China Tel.: +86-551-62901457; fax: +86-551-62901362 E-mail: hfxiang@hfut.edu.cn (H.F. Xiang). ycwu@hfut.edu.cn (Y.C. Wu)
[b] Department of Chemistry & Chemical Engineering, Anqing Normal University, Anhui Anqing, 246011, PR China
[c] Instrumental Analysis Center, Hefei University of Technology, Hefei, Anhui 230009, PR China
[d] State Key Laboratory of Fire Science, University of Science and Technology of China, Anhui Hefei 230026, PR China

1. J. Yang, F. Cheng, X. Zhang, H. Gao, Z. Tao and J. Chen, *J. Mater. Chem. A*, 2014, **2**, 1636-1640.
2. N. Yabuuchi, K. Yoshii, S.-T. Myung, I. Nakai and S. Komaba, *J. Am. Chem. Soc.*, 2011, **133**, 4404-4419.
3. F. Cheng, Y. Xin, J. Chen, L. Lu, X. Zhang and H. Zhou, *J. Mater. Chem. A*, 2013, **1**, 5301-5308.
4. Y.S. Jung, P. Lu, A.S. Cavanagh, C. Ban, G.-H. Kim, S.-H. Lee, S.M. George, S.J. Harris and A.C. Dillon, *Adv. Energy Mater.*, 2013, **3**, 213-219.
5. E. Prada, D. Di Domenico, Y. Creff, J. Bernard, V. S. Moynot and F. Huet, *J. Electrochem. Soc.*, 2012, 159, A1508-A1519.
6. J.-H. Lee, S. Lee, U. Paik and Y.-M. Choi, *J. Power Sources*, 2005, **147**, 249-255.
7. Y. Jiang, Z. Yang, W. Luo, X.-L. Hu, W.-X. Zhang and Y.-H. Huang, *J. Mater. Chem.*, 2012, **22**, 14964-14969.
8. M.M. Thackeray, S.-H. Kang, C.S. Johnson, J.T. Vaughey, R. Benedek and S.A. Hackney, *J. Mater. Chem.*, 2007, **17**, 3112-3125.
9. C.S. Johnson, N. Li, C. Lefief and M.M. Thackeray, *Electrochem. Commun.*, 2007, **9**, 787-795.
10. J. Liu and A. Manthiram, *J. Mater. Chem.*, 2010, **20**, 3961-3967.
11. S. Hy, F. Felix, J. Rick, W.-N. Su and B.J. Hwang, *J. Am. Chem. Soc.*, 2014, **136**, 999-1007.
12. M. Bettge, Y. Li, B. Sankaran, N.D. Rago, T. Spila, R.T. Haasch, I. Petrov and D.P. Abrahama, *J. Power Sources*, 2013, **233**, 346-357.
13. Q.G. Zhang, T.Y. Peng, D. Zhan and X.H. Hu, *J. Power Sources*, 2014, **250**, 40-49.
14. A.R. Armstrong, M. Holzapfel, P. Novák, C.S. Johnson, S.-H. Kang, M.M. Thackeray and P.G. Bruce, *J. Am. Chem. Soc.*, 2006, **128**, 8694-8698.
15. J.M. Zheng, J. Xiao, M. Gu, P.J. Zuo, C.M. Wang and J.-G. Zhang, *J. Power Sources*, 2014, **250**, 313-318.
16. Z.D. Li, Y.C. Zhang, H.F. Xiang, X.H. Ma, Q.F. Yuan, Q.S. Wang and C.H. Chen, J. Power Sources, 2013, **240**, 471-475.
17. Y.-K. Sun, M.-J. Lee, C.S. Yoon, J. Hassoun, K. Amine and B. Scrosati, *Adv. Mater.*, 2012, **24**, 1192-1196.
18. J.M. Zheng, J. Li, Z.R. Zhang, X.J. Guo and Y. Yang, *Solid State Ionics*, 2008, **179**, 1794-1799.
19. S.J. Shi, J.P. Tu, Y.Y. Tang, X.Y. Liu, Y.Q. Zhang, X.L. Wang and C.D. Gu, *Electrochim. Acta*, 2013, **88**, 671-679.
20. I. Bloom, L. Trahey, A. Abouimrane, I. Belharouak, X. Zhang, Q. Wu, W. Lu, D.P. Abraham, M. Bettge, J.W. Elam, X. Meng, A.K. Burrell, C. Ban, R. Tenent, J. Nanda and N. Dudney J. Power Sources, 2014, 249, 509-514.
21. F. Wu, Z. Wang, Y. F. Su, N. Yana, L. Y. Bao and S. Chen, *J. Power Sources*, 2014, 247, 20-25.
22. S.H. Guo, H.J. Yu, P. Liu, X.Z. Liu, D. Li, M.W. Chen, M. Ishida and H.S. Zhou, *J. Mater. Chem. A*, 2014, **2**, 4422-4428.
23. Y. Wu, A.V. Murugan and A. Manthiram, *J. Electrochem. Soc.*, 2008, **155**, A635-A641.
24. J. Cho, Y.-W. Kim, B. Kim, J.-G. Lee and B. Park, *Angew. Chem. Int. Ed.*, 2003, **42**, 1618-1621.
25. J. Cho, J.-G. Lee, B. Kim, T.-G. Kim, J. Kim and B. Park, *Electrochim. Acta*, 2005, **50**, 4182-4187.
26. Q.Y. Wang, J. Liu, A.V. Murugan and A. Manthiram, *J. Mater. Chem.*, 2009, **19**, 4965-4972.
27. S.J. Shi, J.P. Tu, Y.J. Zhang, Y.D. Zhang, X.Y. Zhao, X.L. Wang and C.D. Gu, *Electrochim. Acta*, 2013, **108**, 441-448.
28. K.S. Ryu, S.H. Lee, B.K. Koo, J.W. Lee, K.M. Kim and Y.J. Park, *J. Appl. Electrochem.*, 2008, **38**, 1385-1390.
29. J. Kim, M. Noh, J. Cho, H. Kim and K.-B. Kim, *J. Electrochem. Soc.*, 2005, **152**, A1142-A1148.
30. P. Mohan and G.P. Kalaignan, *J. Nanosci. Nanotechno.*, 2014, **14**, 5028-5035.
31. W. Quan, Z. Tang, J. Zhang and Z. Zhang, *Mater. Chem. Phys.*, 2014, **147**, 333-338.
32. H.Y. Xu, S. Xie, N. Ding, B.L. Liu, Y. Shang and C.H. Chen, *Electrochim. Acta*, 2006, **51**, 4352-4357.
33. H.F. Xiang, H. Wang, C.H. Chen, X.W. Ge, S. Guo, J.H. Sun and W.Q. Hu, *J. Power Sources*, 2009, **191**, 575-581.
34 L. Li, X. Zhang, R. Chen, T. Zhao, J. Lu, F. Wu and K. Amine, *J. Power Sources*, 2014, **249**, 28-34.
35. A. M. Venezia, Catal. Today, 2003, **77**, 359-370.
36. C. Larese, F.C. Galisteo, M.L. Granados, R.M. López, J.L.G. Fierro, P.S. Lambrou and A.M. Efstathiou, *Appl. Catalysis B*, 2004, **48**, 113-123.
37. W.B. Bu, Z.L. Hua, H.R. Chen and J.L. Shi, *J. Phy. Chem. B*, 2005, **109**, 14461-14464.
38. H.Z. Zhang, Q.Q. Qiao, G.R. Li, S.H. Ye and X.P. Gao, *J. Mater. Chem.*, 2012, **22**, 13104-13109.
39. X. Zhang, D. Luo, G. Li, J. Zheng, C. Yu, X. Guan, C. Fu, X. Huang and L. Li, *J. Mater. Chem. A*, 2013, **1**, 9721-9729.
40. C.K. Huang, J.S. Sakamoto, J. Wolfenstine and S. Surampudi, *J. Electrochem. Soc.*, 2000, **147**, 2893-2896.
41. X. Wu, H. Li, H. Fei, C. Zheng, M. Wei, *New J. Chem.*, 2014, **38**, 584-587.
42. X. Yang, X. Wang, Q. Wei, H. Shu, L. Liu, S. Yang, B. Hu, Y. Song, G. Zou, L.Hu, L. Yi, *J. Mater. Chem.*, 2012, **22**, 19666-19672.